ELSEVIER

Physica B 301 (2001) 203–211

PHYSICA B

www.elsevier.com/locate/physb

Superparamagnetic and ferrimagnetic nanoparticles in glass matrix

I.S. Edelman[a,*], R. Ivantsov[a], A. Vasiliev[a], S. Stepanov[b], E. Kornilova[b], T. Zarubina[b]

[a] *L.V. Kirensky Institute of Physics, Russian Academy of Sciences–SB, Krasnoyarsk 660036, Russia*
[b] *S.I. Vavilov Optical State Institute, St. Peterburg 193117, Russia*

Received 13 June 2000; received in revised form 7 December 2000

Abstract

Faraday rotation (FR) spectral, field, and temperature dependencies in oxide glasses with small additions of paramagnetic elements are investigated. Formation of ferrite nanoparticles in amorphous glass matrices is revealed by X-ray diffraction. Particles have crystal structure similar to spinel structure, their dimensions are about 10–24 nm.

The FR field dependencies are typical for ferrimagnetic or superparamagnetic substances depending on particle size. Strong FR increase at the samples cooling (more than twice for some samples) in the temperature interval 105–273 K is observed.

PACS: 75.20.Tt; 78.20.Ls

Keywords: Magnetic nanoparticles; Faraday rotation

1. Introduction

Nano-sized magnetic particles in non-magnetic matrices attract considerable attention because the decrease in the size of particles changes their properties and presents interesting applications for magnetic storage. Different methods of sample preparation lead to the large variety of magnetic behavior observed experimentally in different kinds of systems. Fiorani et al. observed spin glass behavior in the ensemble of iron grains finely dispersed in an amorphous Al_2O_3 matrix, prepared by thin film technology [1]. Tsang and co-authors investigated the ratio of superparamagnetic to high coercivity ferromagnetic particles in the nano-particle ensembles prepared by decomposition of $Fe(CO)_5$ in porous glass [2]. Kodama and co-authors revealed anomalous magnetic properties of organic coated $NiFe_2O_4$ nanoparticles [3]. Superparamagnetic behavior was observed by Babu and co-authors in thin amorphous films $0.5Fe_2O_3$–$0.1Bi_2O_3$–$0.4ZnO$ associated with the ferrite microcrystals formation after films annealing [4].

Recently, we suggested a kalium–alumino–borate glass system containing paramagnetic metal

* Corresponding author. Fax: +7-3912-438923.
E-mail address: ise@iph.krasnoyarsk.su (I. Edelman).

0921-4526/01/$ - see front matter
PII: S0921-4526(01)00274-5

oxide additions in concentrations of several percents mass (for e.g., Refs. [5,6]). In spite of low paramagnetic element concentration nano-sized magnetic particles formed in the glass during the process of the samples additional thermal treatment. As a result, the peculiar magnetic properties of these glasses combined with their transparency in the visible spectral region permitted us to investigate for the first time the magnetooptical Faraday rotation (FR) in the system of nano-sized magnetic particles dispersed in a non-magnetic glass matrix. These glasses were characterized by the non-linear FR field dependence with the hysteresis loops and the saturation in the magnetic fields from 2 to 5 kOe depending on the glass composition and thermal treatment temperature. The remnant FR value, i.e. the FR value in zero magnetic field reached for some samples approximately a half of the FR value in the saturated magnetic field. FR reached high values in different spectral regions depending on the glass composition. For example FR had a spectral maximum near 800 nm, where its value reached $\sim 200\,\mathrm{grad\,cm^{-1}}$ in the magnetic field ~ 1 kOe for glasses containing simultaneously low concentrations of Fe and Co [6]. The combination of properties described makes these glasses prospective candidates for applications in the optical systems of information transmission and processing, especially in the fiber optic technique. It is also worth paying attention to the remnant FR which characterizes the glasses as transparent magnets. Further development of the investigation of this glass system is directed to the enhancement of the FR value in different spectral regions changing the glass composition and thermal treatment conditions. More detailed description of the nanoparticles properties can help to obtain desirable FR dependencies on the external magnetic field. This paper is devoted to the FR and optical density investigation of the glass system containing Fe and Mn oxides together with non-magnetic metal oxides in IR spectral region, including wavelengths 1.3–1.5 μm which are of practical importance now. New approaches to glass preparation provide more homogeneous distribution and minimization of particles sizes in comparison to those presented in our previous papers.

Table 1
Glass compositions, additional thermal treatment temperatures, and the ratio of Mn and Fe molar concentrations $n_2 : n_1$

Glass no.	Composition (% mass)				T treatment (°C)	$n_2 : n_1$
	Fe_2O_3	MnO	Li_2O	BaO		
1	1.5	—	—	—		
2	1.5	0.5	—	—	560	0.37
3	1.5	1.0	—	—	560	0.74
3a	1.5	1.0	—	—	600	0.74
4	1.5	1.5	—	—	560	1.12
4a	1.5	1.5	—	—	600	1.12
5	1.5	0.5	0.10	—	560	0.37
6	1.5	0.5	0.25	—	560	0.37
7	1.5	0.5	—	0.5	560	0.37
7a	1.5	0.5	—	0.5	520	0.37
8	1.5	0.5	—	1.0	560	0.37
8a	1.5	0.5	—	1.0	520	0.37

2. Experimental

KNO_3, Al_2O_3 and H_3BO_3 were used as initial materials to fabricate glasses with the basic composition K_2O–Al_2O_3–B_2O_3. Before synthesis, Fe_2O_3 at a concentration of 1.5% mass and MnO at concentrations from 0.5% to 1.5% mass over 100% mass of the basic composition were added in all glasses. Also, non-magnetic metal oxides which are able to enter, in principle, into ferrite compositions were added in some samples. The sample containing no MnO addition on the one hand and $MnFe_2O_4$ single crystal on the other were investigated for comparison.

Glasses were melted at 1100–1300°C at the oxidation conditions. After being kept at this temperature for 2 h, the glasses were poured onto a steel plate into slabs form about 1 cm in thickness which annealed from a temperature of 380°C. After annealing, an additional thermal treatment of glass samples had been carried out at temperatures from 520°C to 600°C during 3–10 h. Care was taken to see that the additional thermal treatment temperature did not exceed 600°C because higher temperatures led to the crystallization of the basic glass components and to the loss of the glass transparency. Sample compositions and thermal treatment temperatures are presented in Table 1. The

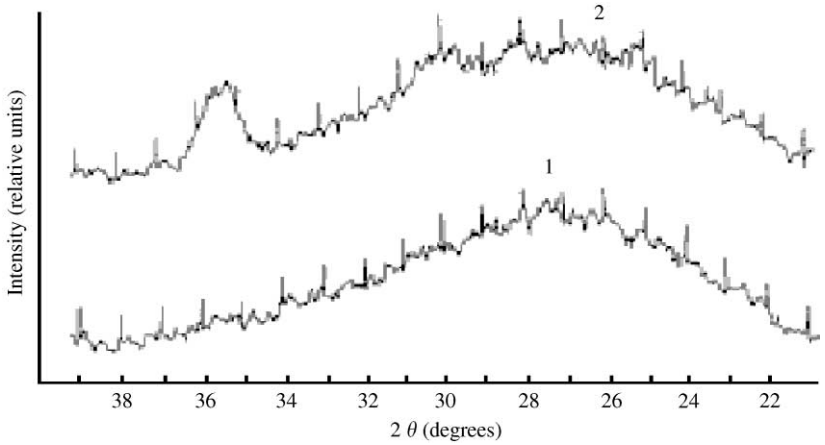

Fig. 1. X-ray diffraction patterns for sample no. 1 containing no Mn additions (1) and sample no. 4 with 1.5% mass MnO (2).

measurements were also carried out for the samples of all compositions which were not subjected to the additional thermal treatment. The measurements were made on optically smoothed samples of (1.0 ± 0.05) mm thickness. The $MnFe_2O_4$ single crystal plate had dimensions of $0.1 \times 3.0 \times 3.0$ mm.

The optical density spectra were obtained with a Hitachi spectrophotometer in the spectral region from the edge of absorption of each sample (900–1000 nm) to 1600 nm. FR was measured with the self-made installation [5] with an accuracy of about 0.2 min in the interval 1000–2000 nm. The external magnetic field was applied normal to the samples surface and changed from -3.5 to -3.5 kOe with an accuracy of ± 20 Oe. Temperature changed in the interval 100–300 K with an accuracy ± 0.5 K. Structural characterization of the glasses was done with a D8ADVANCE (Bruker). X-ray diffraction spectra were recorded for the 2Θ range 5–60° for a Cu K_α emission with $\lambda = 1.5406$ Å.

3. Sample structural characterization

Sample nos. 1 and 2 containing no MnO addition and 0.5% mass MnO without other additions, respectively, were X-ray amorphous (curve 1 in Fig. 1). For all the samples from nos. 3–8a, a distinct Bragg peak centered at $2\Theta = 35.2°$ and essentially weaker peaks at $2\Theta \approx 43°$ and 56° due to crystalline phases were distinguished besides the wide amorphous halo. The part of X-ray diagram for sample no. 4 is shown by curve 2 in Fig. 1. Peak positions for all samples are identical, but peak width and intensity vary from sample to sample. The peaks angle coordinates correspond to the cubic crystal cell. More than that, they correspond to the reflection with the indices (3 1 1), (4 0 0) and (5 1 1) of $MnFe_2O_4$ single crystal. That is why it was enough to measure the angle width of one peak to estimate crystalline size. To eliminate the instrumental contribution to the line broadening the certificate standard sample was used which was the corundum plate with crystallite sizes of (5 ± 2) μm. For this sample the reflection with indices (1 4 0) had the angle coordinate $2\Theta = 35.177°$ and the full width at half maximum (FWHM) $b = 0.208°$. The intense Bragg peak for the samples investigated had the coordinate $2\Theta \approx 35.2°$ and the FWHM B, the latter was essentially larger in comparison to b. The Scherrer equation [7]

$$L = \frac{\lambda}{\beta \cos \Theta}, \tag{1}$$

where $\beta = \sqrt{B^2 - b^2}$, $\lambda = 1.5406$ Å was used to determine average crystalline dimensions. These dimensions are presented in Table 2.

Table 2
Characteristics of the samples investigated[a]

Glass no.	α_0/α_s for 273 K	α_0/α_s for 105 K	α_s (grad cm^{-1}) at 935 nm, 273 K	α_s (grad cm^{-1}) at 935 nm, 105 K	α_s (grad cm^{-1}) at 1500 nm, 273 K	Average particles size (Å)	Q (grad)
3	0.33	0.39	15.94 (8)	25.19 (12.6)	5.00	153	—
3a	0.20	0.31	12.23 (6.1)	21.91 (11)	4.39	137	7.32
4	0.06	0.20	12.86 (4.53)	25.14 (8.4)	5.30	112	—
4a	0.05	0.17	11.67 (3.9)	23.54 (7.8)	6.92	104	12.58
5	0.37	0.38	10.71	15.71	3.34	118	1.07
6	0.41	0.41	11.84	16.94	3.68	183	6.51
7	0.36	0.56	10.50	13.50	2.97	195	5.71
7a	0.14	0.39	5.98	11.18	2.36	118	5.76
8	0.37	0.40	11.50	16.10	3.41	235	7.58
8a	0.26	0.34	5.83	8.83	2.00	161	4.55

[a]The ratio of remnant FR to FR in the maximal magnetic field for two temperatures; FR in the maximal field for two temperatures at 935 nm (in brackets α_s reduced to the MnO concentration equal to 0.5% mass is presented); FR in the maximal field for $\lambda = 1500$ nm at 273 K, average crystalline sizes and figure of merit for $\lambda = 1500$ nm at room temperature. Numbers of samples correspond to those in Table 1.

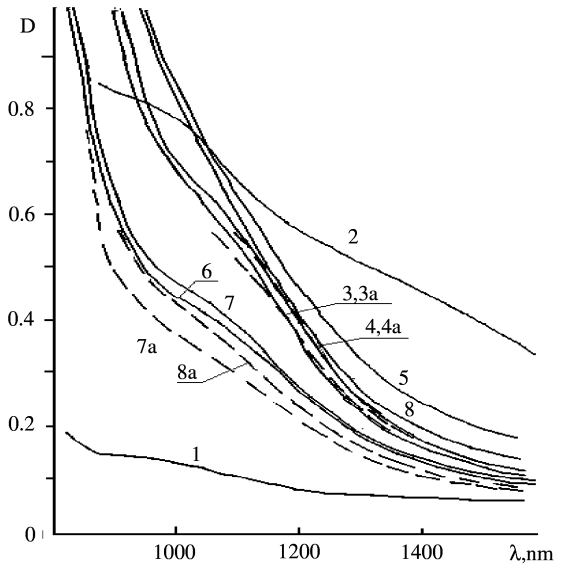

Fig. 2. Optical density curves: numbers correspond to Table 1.

4. Optical density

Spectra of optical density of all samples investigated are presented in Fig. 2. The spectra of initial samples (which were not subjected to the additional thermal treatment) coincide totally with the spectrum of sample no. 1, containing only Fe_2O_3 (curve 1 in Fig. 2). For the conditions used for the glass synthesis, the absorption of the glass did not change after thermal treatment. The additional thermal treatment of glasses containing MnO caused the essential changes of the absorption. Chief among them were the shift of the absorption edge to the infra red (IR) spectral region and an increase of absorption in this region. The strongest increase of absorption was observed for sample no. 2 containing 0.5% mass MnO treated at temperature 560°C. It could evidence the presence of Fe^{2+} ions. Earlier, it was shown [8] that the absorption intensity associated with the Fe^{2+} ions increased strongly when they are incorporated into the magnetic micro- or nanoparticles. The MnO concentration increase was accompanied by the absorption decrease at wavelengths larger than 1000 nm (curves 3, 3a, 4 and 4a in Fig. 2). At the same time, the steepness of the absorption edge near 1000 nm became larger in comparison to sample no. 2 containing 0.5% mass MnO. Besides a kink appears between 1000 and 1100 nm. These changes were practically the same for thermal treatment temperatures both 560°C and 600°C. One of the reasons for such a behavior could be the Fe^{2+} oxidation to Fe^{3+} according to the reaction $Fe^{2+} + Mn^{3+} \rightarrow Fe^{3+} + Mn^{2+}$.

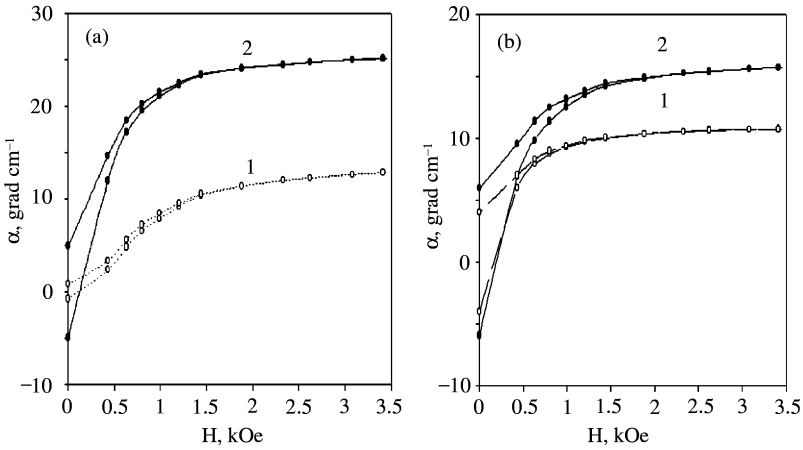

Fig. 3. FR field dependencies for samples (a) no. 4a and (b) no. 5 at 273 K (1) and 105 K (2).

The diamagnetic metal oxide additions Li_2O and BaO into glasses containing 0.5% mass MnO led to the essential changes of absorption spectra. (These oxides themselves have no absorption bands in visible and IR spectral regions and Li and Ba are able to incorporate into ferrite compositions.) The nature of changes is the same for both Li_2O and BaO and coincides with that for glasses with higher MnO concentrations (curves 3 and 4 in Fig. 2). There is a difference between the absorption behavior depending on Li_2O and BaO concentrations. As concerns Li_2O, its concentration increase causes a strong absorption decrease (cf. curves 5 and 6). The BaO concentration increase, in contrast, causes the absorption increase (curves 7 and 8). However, distinctly higher BaO concentration and a small number of concentrations used do not permit the correct comparison between these two cases.

5. Faraday rotation

For all samples FR consists of two contributions: FR of basic glass composition and FR associated with paramagnetic ions. The first one is diamagnetic in nature, has a positive sign and comparatively low value and is characterized by the linear magnetic field dependence. This contribution is independent of the additional thermal treatment. The second contribution is determined experimentally as a difference between the FR value of a given sample and that of the basic glass (i.e. glass containing no paramagnetic additions). This contribution dramatically depends on the additional thermal treatment. Before the treatment it is very low in accordance with the low paramagnetic ion concentration, has a negative sign and is linear on the external magnetic field. These features are typical for the paramagnetic FR. Sample nos. 1 and 2 are characterized by paramagnetic FR and do not change their magnetooptical characteristics after additional thermal treatment. For all the samples from nos. 3–8a listed in Table 1, the treatment leads to FR increase approximately by two orders of magnitude and to the appearance of its non-linear magnetic field dependence.

The typical FR field dependencies are shown in Figs. 3(a) and (b) for sample nos. 4a and 5, respectively, at two temperatures. It is seen that samples differ from each other by FR values in the maximal magnetic field used (α_s) and in zero magnetic field (α_0). We designated the FR value in the maximal field as α_s though this field is not a saturated field as it is seen from Fig. 3. The relation α_0/α_s characterizes the remnant FR value. α_0 and α_0/α_s for two temperatures are presented in Table 2. Comparison of samples with different MnO contents shows no proportionality between FR value and MnO concentration on the one hand and an essential influence of the diamagnetic oxide additions and

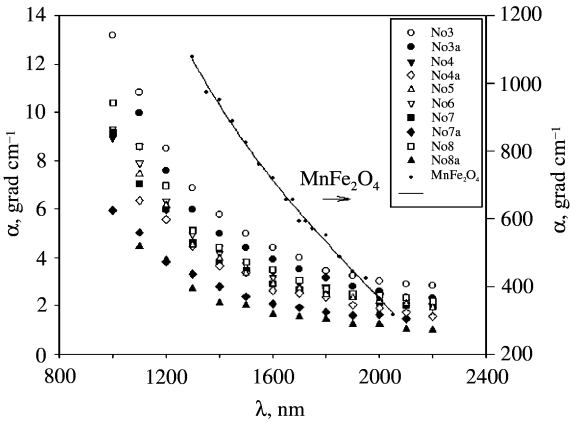

Fig. 4. FR spectral dependencies for the samples presented in Table 2 and for the $MnFe_2O_4$ single crystal plate.

thermal treatment temperature on FR on the other hand. The maximal α_s value reduced to the MnO concentration is observed for sample nos. 6 and 8 containing 0.25% mass Li_2O and 1.0% mass BaO, respectively, and treated at 560°C. The maximal α_0/α_s value for sample no. 6 is observed at room temperature and for sample no. 7 at 105 K.

The measurement temperature decrease in the interval 273–105 K effects the α_s increase for all samples and the α_0/α_s increase for most samples. The α_s increase is practically linear with respect to the measurement temperature. The degree of α_s increase differs for different samples (Table 2): the largest one is observed for sample nos. 4 and 4a. The largest α_0/α_s increase with the temperature decrease is observed for these samples too. For the remaining samples there is no distinct correlation between the α_s and α_0/α_s increase when the temperature decreases.

Magnetooptical figure of merit Q which is determined as the ratio of the FR value to the optical absorption is an important characteristic of a material for technical application. The Q values obtained at the maximal magnetic field used are presented in Table 2 for the practically important wavelength $\lambda = 1.5\,\mu m$. The highest Q is observed for sample no. 4a.

The α_s spectral dependencies are shown in Fig. 4 for all samples. Note that the sign of α_s is negative. Negative FR sign and its graded decrease with the light wavelength increase in the spectral interval presented are characteristic of ferrites with spinel structure containing $3d^5$ magnetic ions (Fe^{3+} and Mn^{2+}).

The FR spectrum measured for $MnFe_2O_4$ single crystal plate magnetized normal to its (1 0 0) surface is presented in Fig. 4 too. It is seen that FR value per unit sample thickness is approximately two orders of magnitude larger for $MnFe_2O_4$ in comparison to the glasses investigated. The rate of the FR value decrease with the wavelength increase is larger for $MnFe_2O_4$ too.

6. Discussion

Magnetooptical properties of the glasses investigated can be associated with the magnetic nanoparticles formation in the glass matrix as a result of an additional thermal treatment. This assumption is based on the X-ray data presented in Table 2 revealing the regions of inhomogeneity in all glasses. These regions have crystal structure which is characteristic of manganese ferrite. The average crystal dimensions vary from sample to sample as it is seen in Table 2. It is possible to propose compositional phase stratification of basic glass components during the process of the additional thermal treatment. Fe, Mn, Li and Ba ions, which can be considered in this case as impurities, displace to the phase boundaries. Thus, regions appear with these elements concentration exceeding strongly their average concentration which provides conditions for the formation of large clusters or nano-sized particles. Indirect exchange interaction through oxygen ions Fe–O–Fe, Mn–O–Mn and Mn–O–Fe in the particles leads to a ferrimagnetic structure appearance similar to that in manganese ferrite. Ferrimagnetic order of the particles is responsible for the high FR value of glasses. The volume concentration of ferrimagnetic particles in glass matrix has to be equal to $\sim 1\%$ in accordance with Fe and Mn molar concentration, which explains the relation between FR value in glasses and in $MnFe_2O_4$ single crystal. It is seen from Table 2 that sample nos. 5–8 demonstrate approximately equal FR values. The relation of Mn and Fe molar concentrations in these samples $n_2 : n_1 \sim 0.37$ which is less in comparison to

$n_2 : n_1 = 0.5$ for the stoichiometric Mn-ferrite. For the samples with higher $n_2 : n_1$ values (nos. 3, 3a, 4, and 4a) the FR value increases insufficiently. Comparing FR values for all samples (excluding 7a and 8a with essentially lower thermal treatment temperature) one can conclude that almost all Fe ions come into particles and only part of the Mn ions corresponding approximately to $n_2 : n_1 \sim 0.5$ are bonding in particles.

It is difficult to understand now the role of diamagnetic metal oxides Li_2O and BaO, but this role is of importance. It is enough to note that samples containing 0.5% mass MnO without Li_2O or BaO additions demonstrate no ferrimagnetic behavior. Besides, these additions influence the optical spectra. According to stoichiometry, $\sim 0.06\%$ mass Li_2O is necessary for the formation of the lithium ferrite phase at the 1.5% mass Fe_2O_3 content in glass. At the same time lithium is bounded very well with the borate glass matrix. So a large amount of Li has to be introduced into the glass composition before it begins to be incorporated into nanoparticles. Our attempts to obtain lithium ferrite particles in the glass containing no MnO additions were unsuccessful. There are two possible variants: Li helps the phase stratification of basic glass composition or it comes to particles which are mixed lithium–manganese ferrites. Similar speculations can be applied to BaO additions. Based on the fact that in the absence of these additions, glasses containing 0.5% mass MnO remain paramagnetic we prefer to assign them some role in the process of the glass phase stratification.

Returning to the FR field dependencies, one can see from Table 2 that there is a definite correlation between the remnant FR value (α_0/α_s) and the temperature FR increase on the one hand and the average particles dimensions on the other. At room temperature, samples with particle dimensions < 130 Å are characterized by the FR field dependence close to the Langevin curve. The average particle dimensions increase causes an increase of the remnant FR value and a decrease of the FR temperature coefficient. Samples nos. 5 and 7a treated at 520°C are exclusions of this regularity: low particle dimensions correspond to the large remnant FR value. This observation needs additional investigation.

As mentioned above, the FR field dependencies for sample nos. 4 and 4a have practically no hysteresis. We tried to describe them in the frame of the theory of non-interacting superparamagnetic particles. The field dependence of the magnetization of an ensemble of such particles is described by the equation

$$M = N\mu V L, \tag{2}$$

where N is the number of particles, μ and V are the saturation magnetization of the particles material and the average particles volume,respectively, L is the Langevin function

$$L = cth\frac{\mu V H}{kT} - \frac{kT}{\mu V H}, \tag{3}$$

where k is the Boltzmann parameter, T is the absolute temperature, H is the external magnetic field. Since FR is a linear function of the magnetization, the shape of the $\alpha(H)$ curve obtained from the experiment will coincide with the shape of the $L(H)$ curve if the magnetic properties of the samples considered are due to the superparamagnetic particles. In the case of close enough coincidence one can estimate the μ value of the nanoparticles material. Such an estimation was realized in the following way. As it is seen from (3) the shape of the $L(H)$ curve depends on the ratio H/H_1, where $H_1 = kT/\mu V$. Several examples are presented in Fig. 5. Note that L is a dimensionless value and it approaches unity when H approaches infinity. To compare the $L(H)$ curve with the experimental $\alpha(H)$ curve, we have to present α as a relative value, i.e. to determine the ratio of α value in definite H, for example, α_s in the maximal H value used in the experiment, to α when H goes to infinity: α_s/α_∞. Varying H_1 and α_s/α_∞ for sample no. 4a we have obtained very close coincidence of the experimental $\alpha_s/\alpha_\infty(H)$ values and calculated $L(H)$ curves with such sets of parameters: $H_1 = 0.131$ kOe and $\alpha_s/\alpha_\infty = 0.92$ at $T = 105$ K and $H_1 = 0.442$ kOe and $\alpha_s/\alpha_\infty = 0.865$ at $T = 293$ K (circles in Fig. 5). Using these H_1 values and the particle volumes given in Table 2 we have obtained μ for sample no. 4a: $\sim 80\,\mathrm{Gs\,cm^3\,g^{-1}}$ for $T = 293$ K and $\sim 105\,\mathrm{Gs\,cm^3\,g^{-1}}$ for 105 K. Both these values are

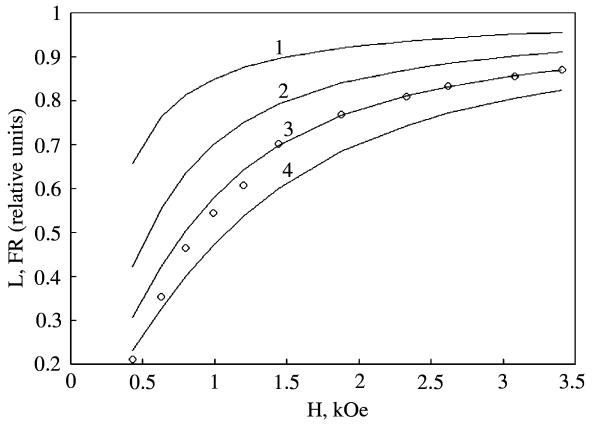

Fig. 5. The calculated field dependencies of L (according to exp.(3)) for different H_1 values: 1–0.15; 2–0.3; 3–0.44 and 4–0.6 kOe. Circles are the relative FR values for sample no. 4a at room temperature.

characteristic of Mn-ferrite [8]. The same results were obtained for sample no. 4. Wider hysteresis loops of other samples prevent the use of this procedure in the whole interval of magnetic fields applied. But the similarity of the FR spectra and X-ray diffraction pattern of all samples allow to suppose the particles composition to be close to Mn ferrite in all cases. Note that we mean a proximity of particles material to Mn ferrite. The deviations of stoichiometry as well as the inclusions of other ions into particle compositions are possible.

An increase of the remnant FR with the decrease of the temperature is probably due to the freezing of the particle magnetic moment. For samples with larger particle dimensions some quantity of particles is in the frozen state at room temperature leading to higher values of the remnant FR.

Strong FR temperature increase exceeding essentially the Mn-ferrite magnetization increase known from Ref. [8] is a more complicated question. The point is that the properties of the ensemble of small magnetic particles can be due not only to the particle composition but also to other factors like, for example, the surface spin disorder considered in Ref. [9]. According to Ref. [9] the influence of this effect on the particles magnetic behavior increases with a decrease of the particle dimensions. The stronger FR value increase with the temperature decrease for the samples with the smaller particle dimensions observed here corresponds to the model [9]. On the other hand, very small particles could have no resulting moment at higher temperatures and give no contribution to FR. The temperature lowering leads to the magnetic moment appearance of such particles. Smaller average particle dimension corresponds to larger amount of particles in an ensemble having no resulting moment at room temperature. In this case, stronger FR increase with the temperature decrease has to be observed also for the samples with the smallest particle dimensions. Probably, other mechanisms can be suggested to explain the FR temperature dependence in the glasses presented. Further investigations are being carried out to elucidate this question.

7. Conclusion

Peculiarities in the FR field and temperature dependencies have been revealed in the glasses investigated. They were explained by the formation of nano-sized particles of Mn-ferrite in amorphous glass matrices. Particle dimensions and structure were determined with X-ray technique

High values of FR and remnant FR in the IR spectral region were observed in some of the samples. The highest magnetooptical figure of merit for the wavelength $\lambda = 1.5\,\mu m$ important for novel practical application was observed for sample no. 4a. For example it was equal to 12.5 grad in the magnetic field 1.0 kOe. The highest FR in zero magnetic field at $\lambda = 1.5\,\mu m$ was equal to $5.3\,grad\,cm^{-1}$ for sample no. 3.

References

[1] D. Fiorani, J. Tholence, J.L. Dormann, J. Phys. C 19 (1986) 5495.
[2] C. Tsang, H.D. Gafney, D. Sunil et al., J. Appl. Phys. 79 (1996) 6025.
[3] R.H. Kodama, J. Magn. Magn. Mater. 200 (1999) 359.
[4] V. Suresh Babu, M.S. Seehra, J. Chen et al., Physica B 212 (1995) 139.
[5] I. Edelman, T. Zarubina, S. Stepanov, T. Kim, J. Magn. Magn. Mater. 110 (1992) 99.

[6] G. Petrovskii, I. Edelman, S. Stepanov, T. Zarubina, T. Kim, Fiz. Chim. Stec. 20 (1994) 748.
[7] L.M. Kovba, V.K. Trunov, X-ray Phase Analysis, Moscow University Publishing House, Moscow, 1976.
[8] J. Smit, H.P.J. Wijn, Ferrites, Philips Technical Library, Eindhoven, The Netherlands, 1959.
[9] R.H. Kodama, A.E. Berkowitz, Phys. Rev. B59 (1999) 6321.